GeoScienceWorld
Lithosphere
Volume 2022, Article ID 3328162, 9 pages
https://doi.org/10.2113/2022/3328162

Lithosphere

Research Article

Numerical Simulation of the Fracture Propagation Mechanism during Supercritical Carbon Dioxide Fracturing in Shale Reservoirs

Fengxia Li,[1,2,3] Tong Zhou,[1,2,3] Haibo Wang,[1,2,3] Jianming He,[4] and Aiping Shi[1,2,3]

[1]*State Key Laboratory of Shale Oil and Gas Enrichment Mechanisms and Effective Development, Beijing 100083, China*
[2]*State Energy Center for Shale Oil Research and Development, Beijing 100083, China*
[3]*Sinopec Petroleum Exploration and Production Research Institute, Beijing 100083, China*
[4]*Institute of Geology and Geophysics Chinese Academy of Sciences, Beijing 100191, China*

Correspondence should be addressed to Tong Zhou; tong_zhou1986@163.com

Received 23 January 2022; Revised 11 October 2022; Accepted 19 October 2022; Published 16 November 2022

Academic Editor: Vincent Heesakkers

To investigate the fracture propagation mechanism during supercritical CO_2 fracturing in shale reservoirs, a numerical model was proposed based on the displacement discontinuity method. The Peng–Robinson equation was introduced to determine the variations in CO_2 properties during the fracturing process. Considering natural fracture distribution in shale reservoirs, the fracture propagation mechanisms during supercritical CO_2 fracturing in shale reservoirs under different horizontal stress differences and matrix permeabilities were analyzed. The influence of the proportion of CO_2 preenergizing on fracture morphology was discussed. The results obtained via numerical simulation show that supercritical CO_2 is beneficial to create a more complex fracture network by activating natural fractures under the same horizontal stress difference. CO_2 easily penetrates into the matrix near the fracture surfaces, increasing reservoir energy. However, when the permeability of shale reservoirs exceeds 0.04×10^{-3} μm^2, substantial filtration of CO_2 into the reservoir matrix occurs near the well bore, limiting the activation of natural fractures around the fracture tip. A higher proportion of CO_2 preenergizing during fracturing is conducive to improve the fracture complexity while reducing the fracture aperture.

1. Introduction

Large-scale hydraulic fracturing is a key technology for the development of unconventional reservoirs, such as shale reservoirs [1–7]. The anhydrous fracturing technology using supercritical CO_2 has attracted much attention because it saves water resources and mitigates the reservoir pollution caused by a conventional water-based fracturing fluid [8–10]. In addition to saving water resources and ensuring environmental protection, supercritical CO_2 has considerable advantages in improving the effect of reservoir stimulation [11, 12]. Supercritical CO_2 has low viscosity and good diffusion, easily entering the microfractures of shale reservoirs, promoting their opening, and forming a more complex fracture network [13]. Conversely, CO_2 dissolves in crude oil, reducing the oil's viscosity and supplementing reservoir energy [14]. However, the phase and physical properties of supercritical CO_2 fracturing are complex, and the mechanism of hydraulic fractures generated by supercritical CO_2 fracturing is still unclear.

Scholars have conducted many laboratory experiments and numerical simulations to study the supercritical CO_2 fracturing mechanisms. Verdon true [14] compared reservoirs stimulated by supercritical CO_2 fracturing as well as hydraulic fracturing and microseismically monitored the fracturing process. Studies have shown that supercritical CO_2 fracturing can achieve the stimulation effect of hydraulic fracturing under the same injection conditions. Li true [15] found that under the same conditions, supercritical CO_2 fracturing has a stronger stimulation effect than hydraulic fracturing. Tsuyoshi et al. [16] performed supercritical CO_2 fracturing experiments with granite and obtained and

reported results similar to those of Verdon true [14]. Zou true [17] integrated the fracturing physical simulation experiment and the acoustic emission monitoring system. The results showed that the acoustic emission events induced by supercritical CO_2 fracturing of tight sandstones were mainly categorized as shear events. [18] used fractal theory to compare the complexity of fractures produced by supercritical CO_2 as well as sliding hydraulic fracturing and demonstrated that the fracture surfaces obtained using supercritical CO_2 as a fracturing fluid were rougher. [19] added pore pressure to the classic fracturing pressure calculation model and found that CO_2 could reduce fracturing pressure. Overall, supercritical CO_2 properties considerably differ from those of the conventional hydraulic fracturing fluids. Moreover, as a fracturing fluid, supercritical CO_2 shows some advantages in reducing fracture initiation pressure and forming complex fractures.

However, current numerical models mainly focus on the influence of low-viscosity CO_2 on the propagation morphology of a single hydraulic fracture [20, 21]. This considerably differs from the complex natural fracture networks of unconventional reservoirs [22–24]. In addition, the physical properties are sensitive to changes in temperature and pressure caused by supercritical CO_2 fracturing [25]. However, existing fracture propagation models often neglect the physical properties of CO_2 to simplify the solving process.

To overcome these challenges, this study establishes a boundary element model suitable for demonstrating fracture propagation mechanism in shale reservoirs based on the displacement discontinuity method (DDM). The Pen–Robinson equation is used to characterize the changes in CO_2 properties caused by temperature and pressure fluctuations during fracturing. Based on the comparison of fracture morphology formed during hydraulic fracturing and supercritical CO_2 fracturing under different reservoir conditions, the influence of the proportion of CO_2 preenergizing on composite fracture propagation is further discussed. The results obtained via this study can provide guidance for the design of supercritical CO_2 fracturing systems.

2. Fracture Propagation Model for Supercritical CO_2 Fracturing

In the process of fracturing, the cross-scale problem from reservoir to fracture is involved, and the strong coupling between solid and liquid is also considered. Therefore, the existing technology is difficult to simulate the mechanical process of fracture network propagation. The displacement discontinuity-boundary element method is to generate grids at fractures, which is more flexible and more accurate than other traditional methods. Therefore, in order to study the mechanism of supercritical CO_2 fracturing in shale reservoirs, a numerical model of fracture propagation in supercritical CO_2 fracturing was established by a displacement discontinuity method. The model assumes that the rock is homogeneously isotropic and that the natural fractures have a minimum opening, allowing fluid to pass through but without stress and deformation. The diffusion of CO_2 in pores and the physical and chemical effects of CO_2 on pores and pore fluids are not considered.

2.1. Solid Equation. Considering the normal and shear displacement discontinuities (DDs) of each fracture element, the total normal and shear stresses caused by the opening and sliding of the fracture system comprising N elements can be given as follows [26]:

$$\begin{aligned}\sigma_n(x) &= \sum_{i=1}^{N}\int_0^{l_i}[G_{11}(x,s)w(s) + G_{12}(x,s)v(s)]K(x,s)ds,\\ \tau_s(x) &= \sum_{i=1}^{N}\int_0^{l_i}[G_{21}(x,s)w(s) + G_{22}(x,s)v(s)]K(x,s)ds,\end{aligned} \tag{1}$$

where $x = (x, y)$ is the coordinate; w and v are the normal and shear DDs, respectively; l_i is the length of fracture i; G_{ij} are the hypersingular Green's functions, which are proportional to the plane strain Young's modulus; σ_n and τ_s are the normal and shear stresses, respectively; and K is the three-dimensional correction coefficient.

To successfully solve the DDM equation in Equation (1), we should first define the boundary conditions. The shear and normal stresses for fracture element i are the boundary conditions, which can be written as follows:

$$\begin{aligned}\sigma_n &= p_i - \sigma_h \sin^2\theta_i - \sigma_H \cos^2\theta_i,\\ \tau_s &= -\frac{1}{2}(\sigma_h - \sigma_H)\sin 2\theta_i,\end{aligned} \tag{2}$$

where σ_h and σ_H represent the minimum and maximum in situ stresses, respectively; θ_i is the angle of the fracture element, moving counterclockwise from σ_h to element i; and p_i represents the fluid pressure acting on element i.

2.2. Flow Equation. Assume that the flow in a fracture satisfies the following equation:

$$q = -\frac{w^3}{12\mu}\nabla p, \tag{3}$$

where q is volume flow rate, μ is viscosity, and w is the opening of the fracture.

The continuity equation that imposes the conservation of mass in one-dimensional flow can be given as follows:

$$\frac{\partial}{\partial t}\left(\frac{\delta v_f}{\delta L}\right) + \nabla q = 0, \tag{4}$$

where v_f is the fluid volume, L is the fracture segment length, and q is the fluid volumetric flux.

Owing to the development of natural fractures in shale reservoirs, numerous randomly distributed natural fractures should be preset in the model. The original permeability of natural fractures usually considerably exceeds that of the shale matrix. Therefore, the natural fractures are assumed to have an initial fracture width w_0, namely, the minimum opening of the element.

2.3. Fracture Propagation Criterion. Based on the theory of fracture mechanics, the following maximum circumferential stress criterion is used to determine the propagation of fracture tip:

$$\frac{1}{2}\cos\frac{\theta_0}{2}\left[K_{\mathrm{I}}(1+\cos\theta_0)-3K_{\mathrm{II}}\sin\theta_0\right]=K_{\mathrm{IC}}, \tag{5}$$

where K_{I} is the stress intensity factor of a type-I fracture, K_{II} is the stress intensity factor of a type-II fracture, and θ is the propagation direction of the fracture tip.

The propagation direction of the fracture tip satisfies the following condition:

$$K_{\mathrm{I}}\sin\theta+K_{\mathrm{II}}(3\cos\theta-1)=0. \tag{6}$$

The stress intensity factors of different fracture modes are estimated by the displacement of the fracture tip element [27].

$$\begin{aligned} K_{\mathrm{I}}&=\frac{0.806G}{4}w\sqrt{\frac{\pi}{l}},\\ K_{\mathrm{II}}&=\frac{0.806G}{4}v\sqrt{\frac{\pi}{l}}, \end{aligned} \tag{7}$$

where w and v are the normal and shear displacements of the fracture tip element, respectively, and l is the length of the fracture tip element.

For unopened natural fractures, natural fractures may occur because of shear failures. According to the Mohr–Coulomb criterion, when a shear failure occurs, it satisfies the following condition:

$$|\tau|\le\mu_f(\sigma_n-p), \tag{8}$$

where τ is the shear stress on the closed fracture surface, μ_f is friction coefficient for fractured surfaces, σ_n is normal stress on closed fracture surfaces, and p is fluid pressure in fractures.

2.4. Physical Properties of CO_2. During supercritical CO_2 fracturing, with the change in temperature and pressure, the density and viscosity of CO_2 will considerably change, further affecting the fracture propagation.

In this study, the Peng–Robinson equation is used to describe the change in the density of CO_2 [28, 29]. The Peng–Robinson equation for CO_2 can be expressed as follows:

$$p=\frac{8.314T}{V-26.667}-\frac{396306.77\times\left[1+0.707979\left(1-\sqrt{T_r}\right)\right]^2}{V(V+26.667)+26.667(V-26.667)}, \tag{9}$$

where T and V are the absolute temperature and molar volume of CO_2, respectively, and T_r is the relative temperature, which is the ratio of absolute temperature T to critical temperature Tc, for CO_2, Tc = 304.13 K.

After the volume of CO_2 is determined according to Equation (9), the CO_2 density under this temperature and pressure can be further obtained.

The viscosity (η) of CO_2 is determined using a previous study [29].

$$\begin{cases} \eta=\dfrac{36.344\eta^*\sqrt{MT_c}}{\sqrt[3]{V_c^2}},\\ \eta^*=\dfrac{\sqrt{T^*}}{\Omega_u}\left\{F_c\left[\dfrac{1}{G_2}+E_6y\right]\right\}+\eta^{**},\\ T^*=1.2593T_r,\\ F_c=1-0.2756\omega+0.059035\mu_r^4+\psi,\\ y=\dfrac{\rho V_e}{6},\\ G_1=\dfrac{1-0.5y}{(1-y)^3},\\ G_2=\dfrac{E_1[1-\exp(-E_4y)]/y+E_2G_1\exp(E_5y)-E_3G_1}{E_1E_4+E_2+E_3},\\ \eta^{**}=E_7y^2G_2\exp\left(E_8+\dfrac{E_9}{T^*}+\dfrac{E_{10}}{T^{*2}}\right),\\ E_i=f_i(\omega,\psi)\quad i=1,2,3,\cdots,10, \end{cases} \tag{10}$$

where M is the molar mass, V_c is the critical volume of CO_2, Ω_u is the collision integral, μ_r is the reduced dipole moment, ω is the acentric factor, ψ is the associate factor for high polar substances, and ρ is the mole number per unit volume.

Based on the aforementioned basic equations, we can describe the changes in physical parameters during the supercritical CO_2 fracturing and analyze their influence on fracture propagation. The model, shown in Figure 1, is solved using MATLAB.

The modeling method was verified and validated; the details had been already discussed in our previous studies [19, 30].

3. Fracture Propagation Simulation

The 200 m × 200 m geometric model established in this study is depicted in Figure 2. Two sets of orthogonal natural fractures are present in the model (short blue lines in Figure 2). In the model, the angle between the direction of the long natural fractures and the maximum principal stress is 0.4π. The injection point is located at the center of the model. Under the simulated displacement of 10 m^3/min, the injection rate obtained according to the simulated reservoir thickness of 50 m is 0.2 m^3/(min·m). The elastic modulus of the shale matrix is 23 GPa, Poisson's ratio is 0.25, and the critical stress intensity factor of type-I fractures is 1.0 MPa·$m^{1/2}$. The horizontal minimum principal stress is 40 MPa along the x-axis, and the horizontal maximum principal stress is 42.5–52.5 MPa along the y-axis.

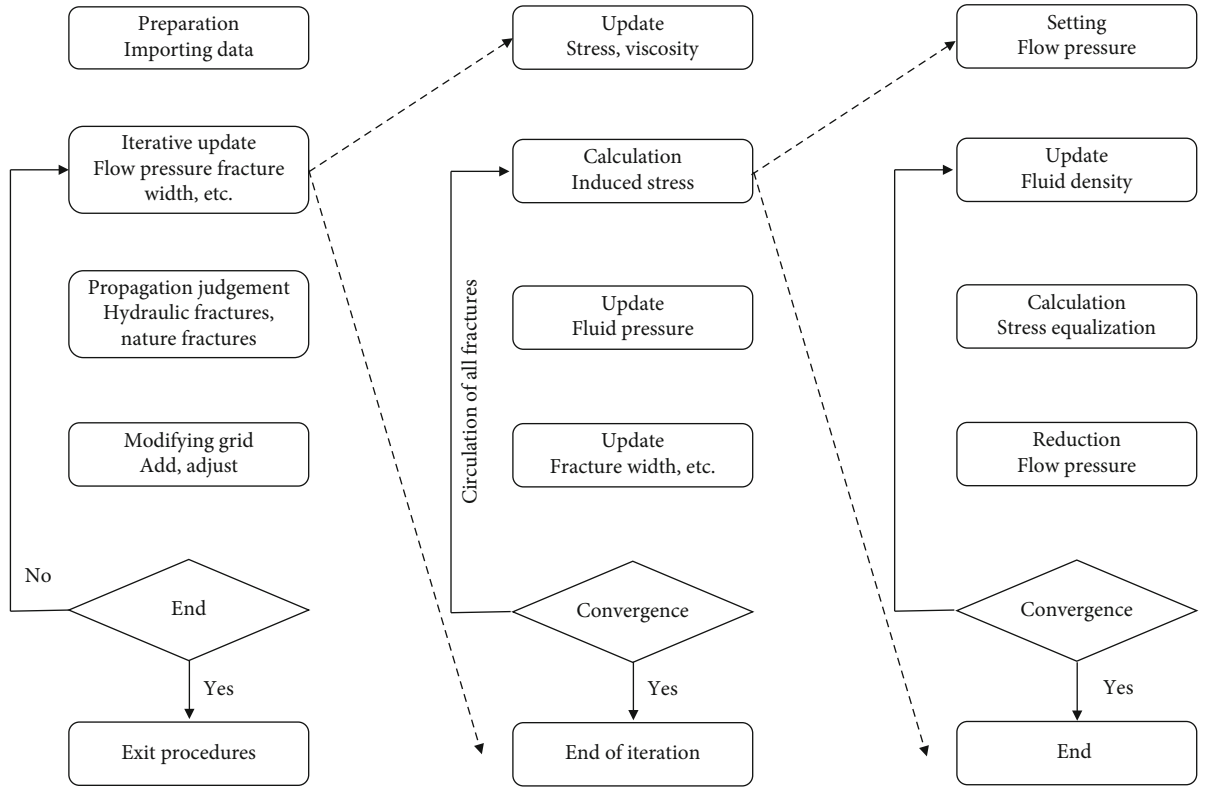

Figure 1: The calculation flowchart of fracture propagation model.

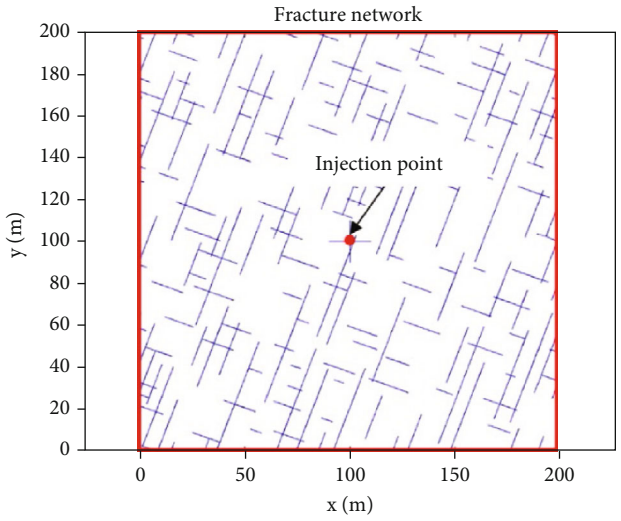

Figure 2: Geometric model.

3.1. Influence of Horizontal Stress Difference. Horizontal stress difference is crucial in the activation of natural fractures. When considering the influence of horizontal stress difference on fracture propagation, the reservoir matrix permeability is set to 0.04×10^{-3} μm^2. Under the conditions of horizontal stress differences of 2.5, 5.0, 7.5, and 12.5 MPa, the results obtained via fracture morphology simulation of slick water fracturing as well as supercritical CO_2 fracturing are shown in Figure 3.

Figure 3 shows that the fracture morphology of shale is jointly controlled by in situ stress and natural fracture distribution. The long-axis direction of the fracture network is roughly along the direction of the horizontal maximum principal stress. The complexity of the fracture morphologies generated by both fluids decreases with the increasing horizontal stress difference. When slick water is used for fracturing, under horizontal stress differences of 2.5 and 5 MPa, the main fractures connect with several natural fractures and deflect laterally to form multibranch fractures (Figures 3(a) and 3(b), left). When the horizontal stress difference exceeds 5 MPa, the number of branch fractures is considerably reduced (Figure 3(c), left) and gradually transforms to a single morphology of hydraulic fractures (Figure 3(d), left).

Under the same horizontal stress difference, supercritical CO_2 fracturing can considerably improve the complexity of fractures. This is mainly because supercritical CO_2 easily enters the matrix pores as well as induced fractures and promotes breaking the matrix and the opening of induced fractures, thereby increasing the number of branch fractures and forming a complex fracture network. Compared with slick water, supercritical CO_2 can more effectively overcome the influence of the high stress difference of 7.5 MPa and form two roughly parallel branch fractures (Figure 3(c), right).

In addition, owing to the differences in fluid properties, the distribution of fluid pressure is different. Slick water with relatively high viscosity has difficulty filtering into the matrix and induced fractures. Therefore, the fluid pressure after

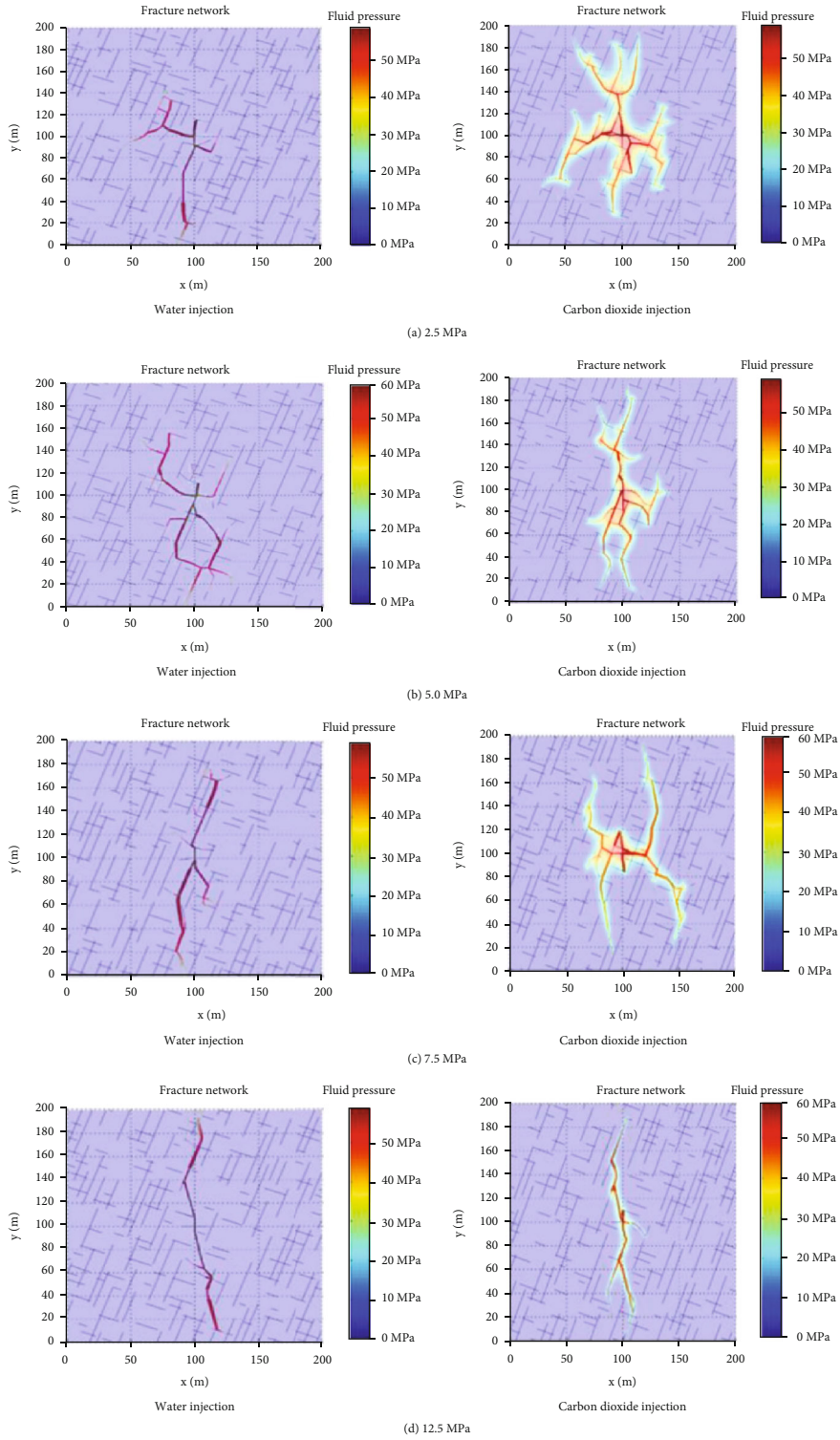

Figure 3: The influence of horizontal stress difference on fracture morphology.

fracturing is mainly distributed inside the hydraulic fractures. Considering Figure 3(a) as an example, the fluid pressure in the shale matrix around the hydraulic fractures and unopened natural fractures considerably increased.

The aforementioned differences show that the filtration effect in supercritical CO_2 fracturing is more apparent than that in slick water hydraulic fracturing. The effect of CO_2 filtration on the fracturing has two mechanisms. CO_2 filtration into the matrix and microfractures reduces the effective stress of the surrounding rock, promoting the fracture of the matrix and the opening of microfractures, thereby reducing the fracture and operating pressures. At the same time, it

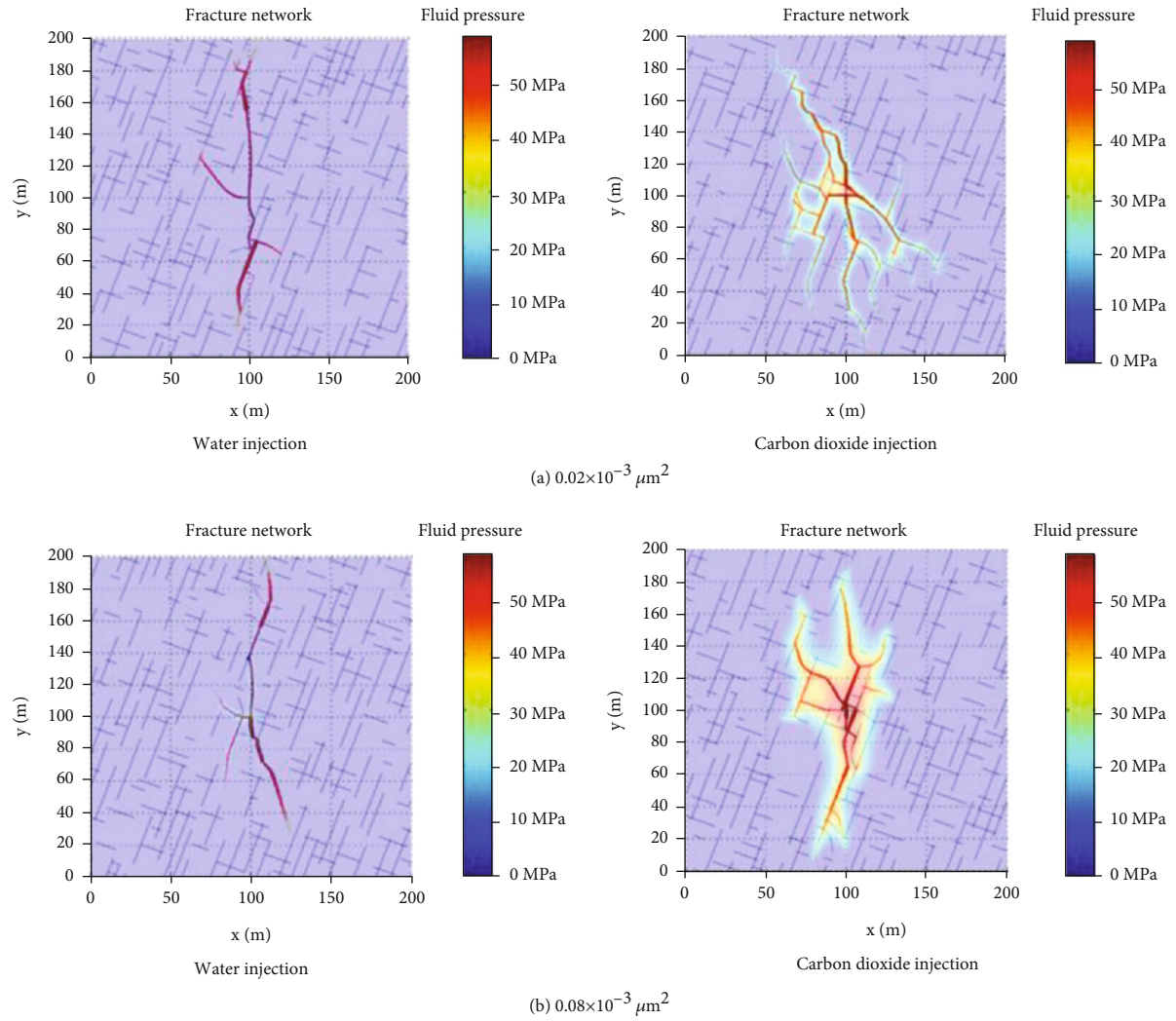

FIGURE 4: The effect of reservoir permeability on fracture morphology.

can increase reservoir energy and reduce oil viscosity. Conversely, the filtration of CO_2 yields a lower fluid pressure in the fractures and smaller fracture openings, thus affecting the fracture efficiency of fracturing fluid.

3.2. Influence of the Reservoir Matrix Permeability. The filtration of CO_2 is closely associated with the reservoir matrix permeability. For a horizontal stress difference of 5 MPa, the fracture propagation was simulated under three matrix permeabilities (0.02×10^{-3} μm^2, 0.04×10^{-3} μm^2, and 0.08×10^{-3} μm^2). When the matrix permeability is 0.04×10^{-3} μm^2, see Figure 3(b). For slick water fracturing, caused by the relatively high fluid viscosity, the filtration rate increases slightly with the increase in permeability; however, the filtration effect is not obvious. The reservoir matrix permeability has little effect on the fracture morphology; thus, the fluid pressure is still relatively high and exerted mainly inside the fractures. Under the same reservoir matrix permeability, the filtration effect of supercritical CO_2 considerably exceeded that of water. As shown in Figure 4(a), when the reservoir matrix permeability is 0.02×10^{-3} μm^2, the filtration of CO_2 into the matrix around the fractures is weak and the influence range is narrow. At the same time, CO_2 can propagate to the far well along the main fracture and open natural fractures at greater distances. When the reservoir matrix permeability is 0.08×10^{-3} μm^2, the filtration of CO_2 into the matrix increases and there is an obvious high-pressure area near the well. In addition, CO_2 easily opens natural fractures near wells but is less effective at opening natural fractures at greater distances.

3.3. Influence of the Proportion of CO_2 Preenergizing on Composite Fracturing. CO_2 composite fracturing is a new fracturing technology used in tight oil and gas reservoirs. It combines the advantages of hydraulic fracturing and CO_2 fracturing. CO_2 preenergizing promotes the activation of natural fractures and increases the complexity of fractures. The proportion of CO_2 preenergizing in composite fracturing affects the fracture network. Therefore, different CO_2 preenergizing proportion is simulated and the results are shown in Figure 5.

Figures 5(a) and 5(b) show that when the proportion of CO_2 preenergizing is low (≤40%), only a few natural fractures

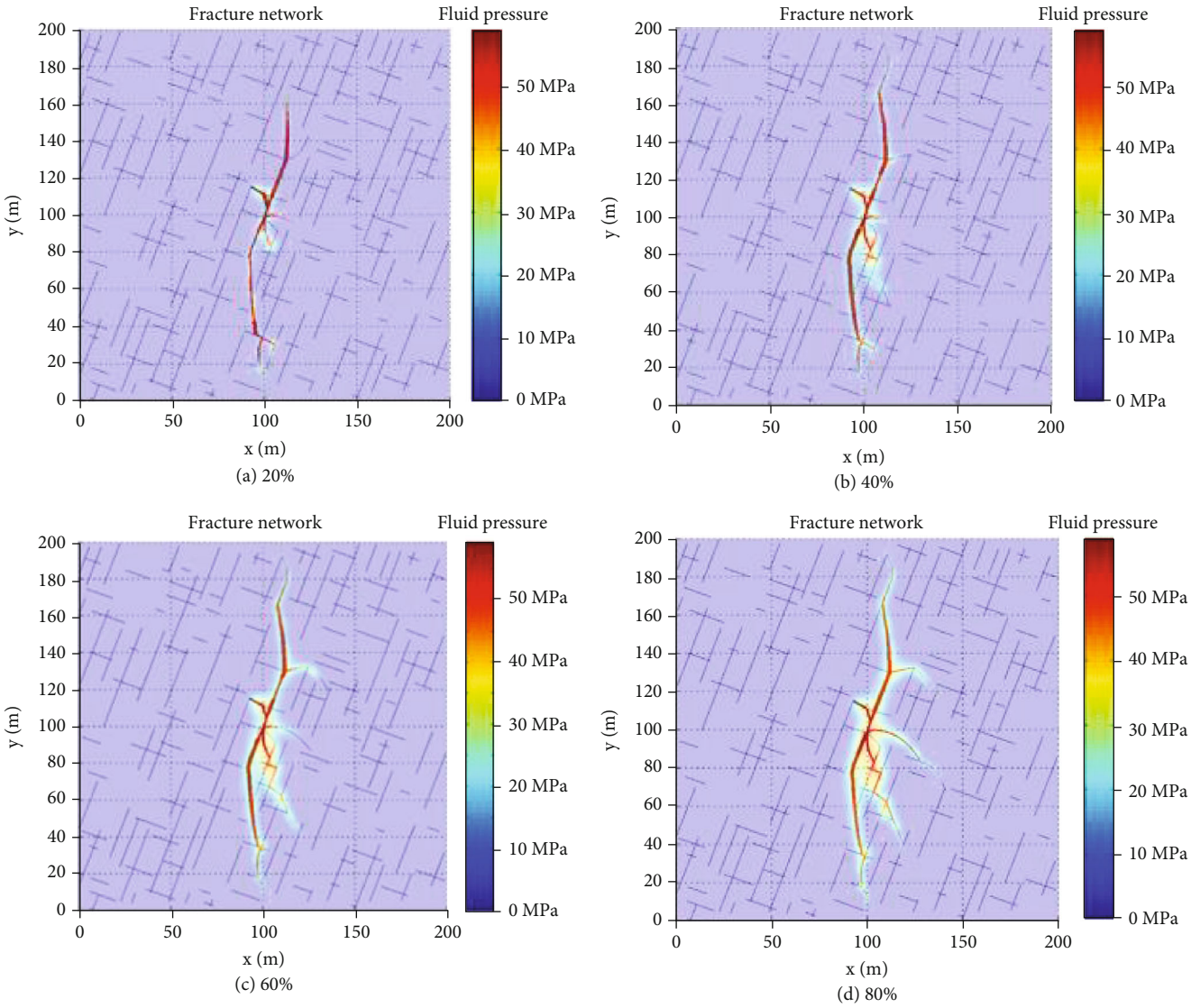

Figure 5: The effect of CO2 preenergizing proportion on fracture morphology.

are activated near the well because of the decreased CO_2 injection. The final fracture morphology is relatively simple, and the statistical fracture lengths are 273 and 319 m, respectively. However, at this time, the fracture openings are larger and the average fracture aperture can reach 2.8 mm and 2.5 mm. In addition, the high-pressure area is mainly distributed across a small range near the well because of CO_2 filtration. As the proportion of CO_2 preenergizing increases, the number of opened natural fractures and branched fractures considerably increases. The statistical results associated with the fracture length show that when the proportions of CO_2 preenergizing are 60% and 80%, the total lengths of fractures are 346 and 389 m, respectively. Furthermore, the reservoir matrix near the fracture shows a fluid pressure increase. However, owing to the decrease in injected water in the later stages and the diversion of branch fractures, the average fracture aperture is considerably reduced to approximately 2.1 and 1.8 mm, respectively.

Overall, under the same reservoir stimulated scope, increasing the proportion of CO_2 preenergizing in composite fracturing improves fracture complexity and expands the range of pressure propagation in the reservoir. However, it limits the opening of fracturing fractures, curtailing the migration of proppant in fractures and thereby reducing the effectiveness of fracturing fractures. Therefore, the proportion of CO_2 preenergizing according to the specific reservoir conditions and the sand required for fracturing should be optimized.

4. Conclusions

(1) When considering the same horizontal stress difference, supercritical CO_2 is more likely to promote the activation of natural fractures than slick water and improve the complexity of the fractures. The low viscosity and easy diffusibility of supercritical

CO_2 are conducive to improving the fluid pressure of the matrix near the fracture surface and increasing the reservoir energy

(2) When the reservoir matrix permeability is low ($0.02 \times 10^{-3}\ \mu m^2$), the supercritical CO_2 filtration effect is weak and it spreads easily along the fracturing fracture to the far well, opening the natural fracture near the fracture tip. When the reservoir matrix permeability is high ($\geq 0.04 \times 10^{-3}\ \mu m^2$), the near-well area has severe filtration, the fluid pressure in the matrix increases considerably, and the natural fracture opening near the fracture tip is limited

(3) Increasing the CO_2 preenergizing proportion in composite fracturing is conducive to increasing the number of natural fractures connected by hydraulic fractures and improving the complexity of fracture network while reducing the fracture opening widths

Data Availability

Data will be available on request.

Conflicts of Interest

The authors declare that there are no conflicts of interest.

Acknowledgments

This study was supported by the project from Sinopec Key Laboratory of Shale Oil/Gas Exploration and Production Technology (33550000-21-ZC0613-0311).

References

[1] F. Dou, J. Wang, C. Leung, and Z. Ma, "The alterations of critical pore water pressure and micro-cracking morphology with near-wellbore fractures in hydraulic fracturing of shale reservoirs," *Engineering Fracture Mechanics*, vol. 242, article 107481, 2021.

[2] L. Huang, G. Sheng, S. Li et al., "A review of flow mechanism and inversion methods of fracture network in shale gas reservoirs," *Geofluids*, vol. 2021, Article ID 6689698, 10 pages, 2021.

[3] D. Jarvie, R. M. Pollastro, R. J. Hill, K. Bowker, B. Claxton, and J. Burgess, "Evaluation of hydrocarbon generation and storage in the Barnett shale, Ft. Worth Basin, Texas," in *Ellison Miles Memorial Symposium*, pp. 22-23, Farmers Branch, Texas, USA, 2004.

[4] G. L. Sheng, Y. L. Su, and W. D. Wang, "A new fractal approach for describing induced-fracture porosity/permeability/ compressibility in stimulated unconventional reservoirs," *Journal of Petroleum Science and Engineering*, vol. 179, pp. 855–866, 2019.

[5] C. Wang and J. Wang, "Effect of heterogeneity and injection borehole location on hydraulic fracture initiation and propagation in shale gas reservoirs," *Journal of Natural Gas Science and Engineering*, vol. 96, article 104311, 2021.

[6] H. Zhao, G. Sheng, L. Huang et al., "Application of lightning breakdown simulation in inversion of induced fracture network morphology in stimulated reservoirs," in *International Petroleum Technology Conference*, 2021.

[7] Z. Zhang, X. Li, J. He, Y. Wu, and G. Li, "Numerical study on the propagation of tensile and shear fracture network in naturally fractured shale reservoirs," *Journal of Natural Gas Science and Engineering*, vol. 37, pp. 1–14, 2017.

[8] H. Liu, F. Wang, J. Zhang, S. Meng, and Y. Duan, "Fracturing with carbon dioxide: application status and development trend," *Petroleum Exploration and Development*, vol. 41, no. 4, pp. 513–519, 2014.

[9] X. Wang, J. Wu, and J. Zhang, "Application of CO_2 fracturing technology for terrestrial shale gas reservoirs," *Natural Gas Industry*, vol. 34, no. 1, pp. 64–67, 2014.

[10] T. Zhou, H. Wang, F. Li, Y. Li, Y. Zou, and C. Zhang, "Numerical simulation of hydraulic fracture propagation in laminated shale reservoirs," *Petroleum Exploration and Development*, vol. 47, no. 5, pp. 1117–1130, 2020.

[11] A. Gupta, A. Gupta, and J. Langlinais, "Feasibility of supercritical carbon dioxide as a drilling fluid for deep underbalanced drilling operations," in *SPE Annual Technical Conference and Exhibition*, Dallas, Texas, 2005.

[12] R. Middleton, J. Carey, R. Currier et al., "Shale gas and non-aqueous fracturing fluids: opportunities and challenges for supercritical CO_2," *Applied Energy*, vol. 147, pp. 500–509, 2015.

[13] A. Abedini and F. Torabi, "On the CO_2 storage potential of cyclic CO_2 injection process for enhanced oil recovery," *Fuel*, vol. 124, pp. 14–27, 2014.

[14] J. Verdon, J. Kendall, and S. Maxwell, "A comparison of passive seismic monitoring of fracture stimulation from water and CO_2 injection," *Geophysics*, vol. 75, no. 3, pp. MA1–MA7, 2010.

[15] G. Li, H. Wang, Z. Shen, S. Tian, Z. Huang, and Y. Cheng, "Application investigations and prospects of supercritical carbon dioxide jet in petroleum engineering," *Journal of China University of Petroleum (Edition of Natural Science)*, vol. 37, no. 5, pp. 76–80, 2013.

[16] T. Ishida, K. Aoyagi, T. Niwa et al., "Acoustic emission monitoring of hydraulic fracturing laboratory experiment with supercritical and liquid CO_2," *Geophysical Research Letters*, vol. 39, no. 16, 2012.

[17] Y. Zou, N. Li, X. Ma, S. Zhang, and S. Li, "Experimental study on the growth behavior of supercritical CO_2-induced fractures in a layered tight sandstone formation," *Journal of Natural Gas Science and Engineering*, vol. 49, pp. 145–156, 2018.

[18] S. Li, S. Zhang, X. Ma et al., "Coupled physical–chemical effects of CO_2 on rock properties and breakdown during intermittent CO_2-hybrid fracturing," *Rock Mechanics and Rock Engineering*, vol. 53, no. 4, pp. 1665–1683, 2020.

[19] X. Zhang, Y. Lu, J. Tang, Z. Zhou, and Y. Liao, "Experimental study on fracture initiation and propagation in shale using supercritical carbon dioxide fracturing," *Fuel*, vol. 190, pp. 370–378, 2017.

[20] J. Edlebeck, G. F. Nellis, S. A. Klein, M. H. Anderson, and M. Wolf, "Measurements of the flow of supercritical carbon dioxide through short orifices," *The Journal of Supercritical Fluids*, vol. 88, pp. 17–25, 2014.

[21] C. Zou, Z. Yang, S. Tao et al., "Continuous hydrocarbon accumulation over a large area as a distinguishing characteristic of unconventional petroleum: the Ordos Basin, North-Central China," *Earth-Science Reviews*, vol. 126, pp. 358–369, 2013.

[22] E. Fathi and I. Y. Akkutlu, "Multi-component gas transport and adsorption effects during CO_2 injection and enhanced shale gas recovery," *International Journal of Coal Geology*, vol. 123, pp. 52–61, 2014.

[23] S. Ha, J. Choo, and T. Yun, "Liquid CO2 fracturing: effect of fluid permeation on the breakdown pressure and cracking behavior," *Rock Mechanics and Rock Engineering*, vol. 51, no. 11, pp. 3407–3420, 2018.

[24] F. Liu, K. Ellett, Y. Xiao, and J. A. Rupp, "Assessing the feasibility of CO_2 storage in the New Albany Shale (Devonian-Mississippian) with potential enhanced gas recovery using reservoir simulation," *International Journal of Greenhouse Gas Control*, vol. 17, pp. 111–126, 2013.

[25] J. Lee, A. Dhuwe, S. D. Cummings et al., "Polymeric and small molecule thickeners for CO_2, ethane, propane and butane for improved mobility control," in *SPE Improved Oil Recovery Conference*, Tulsa, Oklahoma, USA, 2016.

[26] F. Shieibani and J. Olson, "Stress intensity factor determination for three-dimensional crack using the displacement discontinuity method with applications to hydraulic fracture height growth and non-planar propagation paths," in *ISRM International Conference for Effective and Sustainable Hydraulic Fracturing*, Brisbane, Australia, 2013.

[27] K. Wu and J. E. Olson, "Simultaneous multifracture treatments: fully coupled fluid flow and fracture mechanics for horizontal wells," *SPE Journal*, vol. 20, no. 2, pp. 337–346, 2015.

[28] Z. Wang, *Study on characteristics of supercritical carbon dioxide drilling fluid*, China University of Petroleum, 2008.

[29] B. E. Poling, J. M. Prausnitz, and J. P. O'connell, *Properties of gases and liquids*, McGraw-Hill Education, 1987.

[30] J. He, Z. Zhang, and X. Li, "Numerical analysis on the formation of fracture network during the hydraulic fracturing of shale with pre-existing fractures," *Energies*, vol. 10, no. 6, p. 736, 2017.